Laboratory experimental study of ocean waves propagating over a partially buried pipeline in a trench layer

Ke Sun[1, 2], Jisheng Zhang[1, 2], Yuan Gao[1, 2], Dong-sheng Jeng[1, 3], Yakun Guo[2, 4] and Zuodong Liang[3]

[1] State Key Laboratory of Hydrology Water Resources and Hydraulic Engineering, Hohai University, Nanjing 210024, China

[2] College of Harbor, Coastal and Offshore Engineering, Hohai University, Nanjing 210024, China

[3] School of Engineering and Built Environment, Griffith University Gold Coast Campus, Queensland, 4222, Australia

[4] School of Engineering, University of Bradford, Bradford, BD7 1DP, UK

Highlights:

- Provide the first set of comprehensive experimental data for wave-induced pore pressure around a partially backfilled pipeline in a trench layer.
- Systematically investigate the effect of wave characteristics on transient pore-water response in the trench layer near the partial-buried pipeline.
- Integrally examine the effect of trench depth and backfill thickness on oscillatory pore-water pressure around the partial-embedded pipeline.

Abstract: Seabed instability around a pipeline is one of the primary concerns in offshore pipeline projects. To date, most studies focus on investigating the wave/current-induced response within a porous seabed around either a fully buried pipeline or a thoroughly exposed one. In this study, unlike previous investigations, a series of comprehensive laboratory experiments are carried out in a wave flume to investigate the wave-induced pore pressures around a partially embedded pipeline in a trench layer. Measurements show that the presence of the partially buried pipeline can significantly affect the excess pore pressure in a partially backfilled trench layer, which deviates considerably from that predicted by the theoretical approach. The morphology of the trench layer accompanied with the backfill sediments, especially the deeper trench and thicker backfill (i.e.,$b \geq 1\mathrm{D}, e \geq 0.5\mathrm{D}$), provides a certain degree of resistance to seabed instability. The amplitude of excess pore pressure around the trench layer roughly exhibits a left-right asymmetric distribution along the periphery of the pipeline, and decays sharply from the upper layer of the trench to the lower region. Deeper trench depth and thicker buried layer significantly weaken the pore-water pressures in the whole trench area, thus sheltering and protecting the

submarine pipeline against the transient seabed liquefaction.

Keywords: wave-seabed-pipeline interaction; soil response; trenched pipeline; partially buried

1. Introduction

Submarine pipelines, the most widely-used and reliable transportation carrier for offshore oil and gas, are installed in both offshore and nearshore environments with different layouts. They could be laid on the seabed surface, buried in the sediment or embedded in the trench with/without backfilling deposits. Under these conditions, the phenomenon of wave-induced deformation and instability of a porous seabed plays an important role in the design of submarine pipelines because it might potentially compromise the safety of underwater pipelines located either on or in the submarine sediments and result in severe consequences (Christian *et al.*, 1974; Herbich *et al.*, 1984; Palmer and King, 2008; Sumer, 2014a). During cyclic wave loadings, some buried pipeline may float, when the specific weight of the pipeline is smaller than that of surrounded liquefied sediments (Sumer et al., 1999, Damgaard and Palmer, 2001; Damgaard *et al.*, 2006). On the other hand, some pipelines may sink into the seabed when the specific weight of the pipeline is larger than that of the neighboring liquefied deposits (Dunlap *et al.*, 1979; Sumer et al., 1999). Some may even undergo horizontal and vertical displacements after continuous exposure to the wave-current combined actions (Damgaard *et al.*, 2006). Numerous failures of submarine pipelines have been reported to be linked to wave-induced seabed instability which is vulnerable to liquefaction (de Groot and Meigers, 1992; Sumer, 2014b, c). Such failures could be catastrophic during severe storms or hurricanes. Due to its practical engineering importance, the interactions between waves/currents, a seabed and a pipeline have attracted great attentions among geotechnical and coastal engineers. A state-of-art review of recent research on the pipeline-seabed interactions exposed to waves and/or currents can be found in Fredsøe (2016).

When a submarine pipeline is involved, the problem of fluid-seabed interaction becomes more complicated, because the pipeline will disturb local flow field and sediment transport. Numerous investigations for the wave-seabed-pipeline interactions have been carried out since 1970. MacPherson (1978) and McDougal *et al.* (1988) proposed analytical solutions for an infinite seabed, which exhibits perturbations in the pore pressure field around a marine pipe. Monkmeyer *et al.*

58 (1983) developed an algorithm with the concept of "image pipe", which can be applicable to a
59 soil layer of a finite thickness. Magda (1992) extended Okusa's (1985) model to investigate a fully
60 buried pipeline in a seabed by solving the Laplace's equation and consolidation equation.
61 Compared with the previous model without consideration of a submarine pipeline (Okusa, 1985),
62 the perturbation due to existence of a subsea pipeline was included in the model of Magda (1992).

63 In addition to analytical approximations, several numerical models have been proposed for the
64 problem. Among these, Cheng and Liu (1986) applied a boundary integral equation model to solve
65 the wave-induced soil response around a buried pipeline. In their study, the trench is surrounded
66 by two impermeable rigid walls and *u-p* approximation (*u* represents the soil displacement, *p* is
67 the pore-water pressure) is adopted. Magda (1996) considered a similar case with a wider range
68 of the degree of saturation, but based on consolidation model (i.e., quasi-static soil behavior is
69 considered). Jeng and his co-workers applied their two-dimensional finite element model (Jeng,
70 2003) to various conditions with a pipeline, including Gibson soil (Jeng and Lin, 1999), effect of a
71 cover layer (Wang *et al.*, 2000), internal stresses of the pipeline (Jeng, 2001; Jeng *et al.*,2001). The
72 model was extended by Gao *et al.* (2003a) and Gao and Wu (2006) to investigate the cases with
73 non-linear wave loading. Dunn *et al.* (2006), applying the poro-elastoplastic model (Chan, 1988),
74 conducted a systematic investigation of wave-induced soil liquefaction caused by residual pore
75 pressure around a fully embedded pipeline. Luan *et al.* (2008) further considered the contact
76 effects between pipeline and soil with dynamic soil behavior. In their study, three different types
77 of trench layers, i.e., square, rectangular and triangular, were considered. All these studies only
78 considered a fully buried pipeline. Zhao and Jeng (2014) and Zhao *et al.* (2014) were the first
79 attempt for considering a partially buried pipeline in a trench layer with a natural backfilling
80 process. Recently, Zhao and Jeng (2016) further investigated the effects of backfill in trench layer
81 on the seabed liquefaction and proposed a relationship between the critical backfill thickness and
82 wave steepness and other wave and soil characteristics. In their numerical studies, residual
83 liquefaction was considered. Lin *et al.* (2016) developed an integrated FEM to investigate transient
84 liquefaction occurrence nearby the trenched pipeline with different backfill depths. This

framework was further extended to the case subject to combined wave and current loadings in two-dimension and three-dimension (Duan *et al.*, 2017a, b). In these studies (Zhao and Jeng, 2016; Duan *et al.*, 2017a), a simplified approximation process for the design of the critical thickness of backfill depth with given wave characteristics and soil parameters is proposed for the protection of the pipeline against soil liquefaction.

Apart from theoretical approaches and numerical modeling studies, laboratory experiment is another common methodology to reveal the physical process and its mechanism of the wave-soil-structure interactions. In general, three different experimental methods have been reported in the literature. First, one-dimensional compressive tests are conducted in a vertical cylinder (Zen and Yamazaki, 1990a; 1990b; Chowdhury *et al.*, 2006; Liu *et al.*, 2015; Liu and Jeng, 2016). With this experiment set-up, it is possible to install ten or more pore-water pressure transducers in the soil column, which could provide more measurable data to resolve the vertical profile of pore pressure distribution in the seabed, especially in the region near the seabed surface. However, this type of experiment can only capture the response of soil to oscillatory pore pressure in time domain, not in spatial domain, because only oscillatory dynamic pressures are applied at the top of the cylinder and no shear strain is generated in the soil column.

The second type of experimental approach is the geo-centrifugal wave tests (Sassa and Sekiguchi, 1999; 2001; Miyamoto *et al.*, 2004). In this approach, the stress level in the soil at the experimental model under the environment of several times of gravitational acceleration is the same as that of the prototype. This approach can simulate the pore-water pressure fluctuation in both spatial and time domains, although the wave generation in the experiment may not represent the realistic ocean waves and only limited numbers of measurements can be taken. Furthermore, complicated engineering problems such as the current problem with a trench layer cannot be simulated in geo-centrifugal tests.

The third type of experimental approach is wave flume test, which have been commonly used by coastal engineering researchers. Turcotte *et al.* (1984) were the first to conduct experiments for

111 the wave-induced pore-water pressure around a buried pipeline in a wave flume. Sumer *et al.*
112 (1999) carried out a series of laboratory experiments to explore the wave-induced seabed
113 response under progressive waves, and then the sinking/floatation of marine pipelines in the
114 liquefied soil. Sudhan *et al.* (2002) carried out the experimental investigation to analyze wave-
115 induced pressure on a pipeline fully buried in a permeable seabed with different burial depths.
116 They found that high-pressure values took place at the top and low-pressure values appeared at
117 the bottom. Teh *et al.* (2003; 2006) studied the sinking/floatation of pipelines in a liquefied seabed.
118 They demonstrated that the pipeline behavior on a mobile seabed strongly depended on specific
119 gravity of itself and liquefied soil characteristics, but not on the wave parameters. Sumer *et al.*
120 (2006) further extended their experiments to explore the liquefaction due to the buildup of pore
121 pressure around a buried pipeline. Their research work further indicated that the accumulation of
122 pore pressure and the residual liquefaction were influenced by the boundary condition of pipeline
123 surface. In general, liquefaction occurs in the top layer and develops downwards with the absence
124 of the marine pipeline, whereas under the presence of the pipeline, liquefaction occurs at the
125 bottom of the pipeline and develops along the perimeter of the pipeline upwards. Recently, a
126 series of wave flume tests were carried out (Gao *et al.*, 2002; 2003b; 2007; 2011) to examine the
127 fluid-pipeline-seabed interaction mechanism for the lateral stability of un-trenched pipelines as
128 well as partially embedded pipelines for various loading conditions, e.g., the wave action and/or
129 the current action. Pan *et al.* (2007) conducted large-scale wave flume experiments to investigate
130 various parameters on the pore pressure around a submarine pipeline with a shallow burial depth
131 due to regular waves, such as relative water depth, relative burial depth and scattering parameter.
132 Zhou *et al.* (2011) conducted a series of physical modelling tests in wave flume on soil responses
133 with a pipeline either half buried or resting on the seabed under regular waves or combined with
134 currents. Recently, Yang *et al.* (2012a, b; 2014) conducted laboratory experiments to investigate
135 the stability of marine pipeline due to regular and irregular wave-induced scour. They found that
136 attaching a rigid spoiler at the top of the pipeline could greatly accelerate the scour around the
137 pipeline as well as the so-called self-burial (Yang *et al.*, 2012a, b). When a flexible rubber was placed
138 under the pipeline, no scour around the pipeline would occur if the length of the rubber reaches

139 a critical value and the pipeline was protected (Yang *et al.*, 2014).

140 Besides the above experimental approaches, based on some practical projects, such as PIPESTAB
141 Project, DHI Research Program and AGA Project, the interaction between wave-seabed around
142 an unburied-pipeline was investigated by means of mechanical loading tests (Palmer *et al.*, 1988;
143 Allen *et al.*, 1989). In this approach, wave growth process and horizontal propagation is neglected.
144 However, the above physical modelling studies are impossible to simulate the pore pressure in
145 the trench layer around a partially buried pipeline, which can be easily achieved through the wave-
146 flume experiments.

147 In summary, to reproduce the problem of the practical wave-soil-pipeline interaction within a
148 trench layer, wave flume tests seem to be a more appropriate approach, although it has some
149 limitations and shortcomings.

150 The aforementioned studies are primarily concerned with pore-water pressures around an
151 underwater pipeline, either directly resting on the seafloor or shallowly/fully buried in the seabed,
152 in which the soil responses are well acknowledged. While rare attention has been paid to the
153 wave-induced responses of trench layer nearby a partially backfilled pipeline. The complicated
154 seafloor profile combined with the bare pipeline segment will strongly affect the local flow and
155 consequently the sediment transport. However, in the engineering practices, the submarine
156 pipelines are typically deployed in a trench with partially backfill soil to strengthen the stability
157 and reduce costs simultaneously (Du and Zhao, 2015).

158 The first set of experimental data for wave-induced pore pressure around a partial- buried pipeline
159 in a trench layer was reported by Zhai *et al.* (2018). However, in their experiments, only four
160 measuring points were deployed around the periphery of the pipeline in total, in which the pore
161 pressure variation in the trench layer nearby partially embedded pipeline cannot be captured.
162 Therefore, to have a better understanding of the whole physical process and mechanism, a series
163 of comprehensive experiments are desired for pipeline engineers and researchers, which

motivates this study. Main objectives of this paper are to examine the wave-driven pore-water pressure in trench layer around a partially buried pipeline through physical modelling, including:

(i) Providing a comprehensive experimental database for the wave-induced pore-water pressures in the vicinity of a submarine pipeline partially buried in a trench layer.

(ii) Consideration of partially buried pipeline in a trench layer, in which the pore pressure may deviate considerably from that predicted by the poro-elastic models (e.g. Liang and Jeng, 2018a, b);

(iii) Investigation of the effects of wave characteristics on trench layer, where the local flow will be definitely disturbed by the complicated seabed-pipeline configuration;

(iv) Exploration of the effects of backfill thickness and trench depth in the vicinity of the partially embedded pipeline, where the sediment mobility and soil instability would be suppressed.

2. Experimental setup

A series of wave flume tests are carried out to investigate the process of the wave-driven pore-water pressure around a trenched pipeline with partially sediment backfilling. To the authors' best knowledge, this is the first comprehensive experimental work for such a problem in the literature, and expected to provide invaluable data for future studies in the field.

2.1 Facilities and instruments

The experiments are conducted in a wave flume having the dimension of 55 m (long) × 1.3 m (high) × 1.0 m (wide) at Hohai University. As shown in Figure 1, the wave flume is equipped with a hydraulic piston-type wave maker at the upstream end and a sponge-type wave absorber at the downstream end to dissipate the incoming wave energy and thus minimize the wave reflection effect. The wave maker is capable of generating regular waves with wave period of 0.6 sec - 2.5

187 sec and the maximum wave height of 0.2 m. A sediment basin located at a distance of 25 m away
188 from the wave generator with the size of 2.0 m (length) × 1.0 m (width) × 0.58 m (depth), is
189 manufactured for the experiments specifically. The surrounding walls and the bottom of the test
190 sand-pit are made of rigid and impermeable concrete. As shown in Figure 1, the pit is elevated 0.25
191 m in height, based on the original 0.33 m depth, by introducing two artificial trapezoids (false
192 floors) on both ends of the sediment basin. The false floors at each side comprises a 1:10 slope
193 plywood ramp and a 7.5 m-long false floor, keeping off both the generation of reflaction wave
194 and progressive wave deformation to ensure smooth transition of waves to the utmost before
195 propagating through the measurement section.

196 In the experiments, the wave-induced pore-water pressure variation and water surface elevation
197 around a pipeline placed in a backfilled trench are measured simultaneously by using the pore
198 pressure sensors and wave height gauges. The CY203/CY303 type miniature pressure transducers
199 (6 mm in outer-diameter) are designed and manufactured by Chengdu Smart World Technology
200 CO.LTD. The measurement range of the transducer is 30kPa with accuracy of ±0.1% Full Scale.
201 Three pressure transducers are installed to record wave-driven pore-water pressures in the soil
202 along the central line at different depths of 0.23 m, 0.27 m, and 0.40 m below the seabed surface.
203 Another eight pressure transducers, deployed around the pipeline circumference with a fixed
204 interval of $\pi/4$, generally record the hydrodynamic pressure when exposed to water and
205 occasionally obtain the pore-water pressure when buried in the soil. The wave height gauges,
206 designed by Nanjing Hydraulic Research Institute with the measurement range of 0.60 m and the
207 measurment precision of 0.1 mm, are located along the central axis of the wave flume, containing
208 one far-field gauge to measure the incoming wave characteristics and four near-field ones to
209 explore the wave evolution propagating through the porous seabed. A remote computer
210 connected to the servo system and acquisition system is employed to sample the signals of wave
211 height gauges and pore pressure transducers synchromously, with sampling frequency of 50 Hz.
212 The locations of the measurement device are indicated in Figure 1.

2.2 Properties of seabed sediments

The sandy sediment with mean particle size of d_{50}=0.173 mm, is used as the seabed material (for both trench-layer and backfill-layer) in the experiments, and its main physical properties are listed in Table 1. In Table 1, the submerged specific gravity of soil is defined as $\gamma' = (1-n)(\gamma_s - \gamma_w)$ where γ_w is the unit weight of pure water, γ_s represents the unit weight of soil grains and *n* is the soil porosity. The mean grain size and grading curve of sandy sediment is measured with Mastersizer 3000E, while permeability coefficient is measured by the constant head permeability test. Water is introduced into flume and left for 3 days before experiment is run to allow the subsidence of the seafloor is complete and the variation of void ratio is negligible. This is also to ensure the seabed to be almost fully saturate. As mentioned previously, because laboratory experiments can be performed in a wave flume with natural waves/currents, many liquefaction experiments are based on the small-scale wave flume experiments with 1 - g environment rather than N – g environment made by centrifuge tests. The purpose of wave flume tests is mainly to capture the residual pore pressure as well as the response of seabed to pore pressure oscillation. However, the drawback of wave-flume experiments is that the stress level cannot be simulated as the prototype stress level in the seabed. Thus, in the present tests, no scaling law for seabed sediments is adapted, because the model was regarded as a small prototype. The seabed thickness is maintained at 0.58 m for all tests.

2.3 Characteristics of submarine pipeline

A PMMA (polymethyl-methacrylate) pipeline with the external diameter of 0.1 m is used to model the submarine pipeline, as illustrated in Figure 1, laying at the seafloor perpendicularly to the direction of wave propagation. To eliminate the side effects, the pipeline length is chosen to be 0.96 m, slightly smaller than the internal width of wave flume. Therefore, the gap between the end of pipeline and the wall of the flume is too small to generate large score holes and notable flow disturbance. This would simplify the simulation of wave-seabed-structure interaction as a two-dimensional problem. Besides, the pipeline movement is thoroughly constrained through a

steel frame, including translational motion and rotation. As mentioned before, eight pore-water pressure transducers are equally spaced around the pipeline circumference at the center section, as shown in Figure 1.

The weight of the pipeline has been adjusted to model the typical submerged weight of actual pipeline. According to the gravity similarity parameter $G = W_s/\gamma' D^2$ proposed by Gao *et al.* (2003), where W_s is the submerged weight of pipe. Hence, the dimensional analysis of model and prototype can be expressed by $\lambda_G = \frac{\lambda_{W_s}}{\lambda_{\gamma'}\lambda_D^2}$, where λ represents the ratio of the parameters of model to that of prototype. As aforementioned, the model pipe is made of PMMA, with length of 0.96 m, and the outer diameter and inner diameter are 0.1 m and 0.08 m respectively. Herein, the submerged weight of the pipe is 4.985 N/m.

2.4 Conditions of incident waves and soil patterns

Due to the unpredictability and uncertainty of the storm waves, it is difficult to obtain accurate data in the field marine environment. This makes laboratory experiments of pipeline model be of particular importance. Extreme care is taken to make sure that the behavior of model simulates that of the prototype as accurately as possible.

In the wave-seabed-pipeline coupling problem, three non-dimensional numbers relative to flow characteristics can be deduced. They are: (1) the Froude Number $Fr = U_m/\sqrt{gD}$, which represents the ratio of inertia force to gravitational force; (2) the Keulegan-Carpenter Number $KC = U_m T/D$, which controls the generation and development of vortex around pipeline, and is related to the hydrodynamic force acting on the pipe under wave motion, and (3) the Reynolds Number $Re = U_m D/\nu$, which is the ratio of inertia force to viscous force. Here U_m is the flow velocity; D is the pipe diameter; T is wave period and υ is kinematic viscosity of water.

According to the principle of similarity from the Froude number $\lambda_{Fr} = \frac{\lambda_{U_m}}{\lambda_g^{1/2}\lambda_D^{1/2}} = 1$, where λ

represents the ratio of the parameters of model to that of prototype, since $\lambda_{\mathrm{g}} = 1$, the following relationship should be maintained:

$$\lambda_{\mathrm{U_m}} = \lambda_{\mathrm{D}}^{1/2},$$

which could be further rendered to

$$\lambda_{\mathrm{T}} = \frac{\lambda_{\mathrm{D}}}{\lambda_{\mathrm{U_m}}} = \lambda_{\mathrm{D}}^{1/2}.$$

Therefore,

$$\lambda_{\mathrm{KC}} = \frac{\lambda_{\mathrm{U_m}} \lambda_{\mathrm{T}}}{\lambda_{\mathrm{D}}} = 1,$$

This indicates that *Fr* and *KC* numbers can be satisfied concurrently during the model simulation. In the natural marine environment of ocean wave with a free surface, the effective range of viscosity force is restricted to the immediate vicinity around the particles and hardly affects the overall motion of the fluid, hence the viscosity force is negligible while the gravity and inertial force predominates the fluid motion and consequently the interactions of wave-seabed-pipeline. Since *Fr* and *Re* numbers cannot meet the principle of similarity synchronously during the laboratory experiments, it is reasonable to yield the wave-seabed-pipeline couple problem to the scaling law of the Froude number and to make allowance for the deviation in the Reynolds number scale. Small-scale experiments have limited values because the Re is usually much higher in the prototype than in the experiments. The value of Fr and KC numbers of coastal sediments in South China Sea varies between 0-0.5 and 0-20 respectively (Gao et al., 2003), which is within the range used in the present laboratory experiments.

The experimental conditions are listed in Table 2. For a fully buried submarine pipeline (i.e., trench depth *d*=backfill depth *e*), the wave height (*H*) varies from 0.06 m to 0.14 m with an interval of 0.02 m, and the wave period (*T*) ranges from 1.2 sec to 1.8 sec where set 0.2 sec as a span. For the

partially buried pipeline, the incident wave is only adopted as H=0.12 m and T=1.6 sec. The water depth is kept at 0.40 m above the sediment basin for all tests.

Apart from the trench depth, the side slope and bottom width will definitely affect the soil response in the trench soil layer. However, limited by submarine repose angle of model sand particle, the gradient of the trench chosen in this study is 1:2, where trench depth is the dominant factor whereas the bottom width of the trench has the minus impact according to the preliminary understanding. Therefore, this study places priorities on the trench depth as well as the backfill thickness, instead of the side slope and bottom width.

2.5 Test procedures

The procedure of test is as following:

(1) *Place the facilities and instruments:* Eight pore pressure transducers are installed in the drilled holed around the pipeline covered with waterproof tape, and another three are strapped at the steel frame located at the bottom of sediment basin. Four wave height gauges are deployed along the central axis of the wave flume. As the pore-pressure transducers are equipped with sand filters, they must be submerged in water for at least 24 hours to ensure air would be completely exhausted.

(2) *Fulfill the sediment basin:* Prior to the experiments, the large amount of sand is firstly poured into the soil-mixture tank, and water is gradually added into the tank while continuously and thoroughly stirring until it reaches the homogeneous liquid state. The mixture is then pumped into the test section where it is allowed to consolidate for at least 3 days. Finally, a soil layer of about 0.58 m in thickness is produced.

(3) *Place the submarine pipeline:* The trench (1:2 side slope with 0.16 m in bottom width) is dredged via iron plate as soon as the consolidating soil layer surface is leveled with the false floor. The pipeline is then placed at the central bottom of the trench.

(4) *Backfill the trench layer and fill the flume:* The trench is backfilled with prescribed backfill material to an intended thickness. The flume is then filled with clear water as slowly as possible to the designed water depth. Extreme care should be taken to ensure that the soil configuration, especially the turning point from platform to slope, is not washed away. The backfill soil under hydrostatic pressure is left to settle and consolidate for 3 days.

(5) *Switch on the wave maker.*

(6) *Sample the statistics of pore pressure and wave height:* The duration of data collection is at least 120 sec after the oscillatory soil response in sandy seabed is fully developed and reaches to equilibrium state.

(7) *Switch off the wave maker.*

(8) *Empty the wave flume and clean the sand pit.* Repeat step2 to step7 for the next test.

3. Comparison with the numerical model (Liang and Jeng, 2018a, b)

In this section, the laboratory experiment is compared with the previous numerical model for wave-soil interactions around a partially buried pipeline (Liang and Jeng, 2018a, b). In the wave model, the RANS equations are employed to simulate the progressive wave motion over a porous seabed near the trench layer; while in the seabed model, the Biot's consolidation equation is solved to investigate the distribution of pore pressure, effective stress and soil displacement of the seabed in the trench around a partially backfilled pipeline. With the consideration of one-way coupling process, the integrated numeral model is established with the OpenFOAM.

Figure 2 shows the simulated and the measured water surface elevation (η) versus time, recorded by wave height gauges h4, for Test 10 and Test 49. Figure 3 shows the comparison between the simulated and the measured normalized amplitude of excess pore-water pressure ($|u_e|/p_0$) around the outer surface of submarine pipeline (θ) for Test 10 and Test 49. Test 10 is the case of a fully buried pipeline (where trench depth is *d*=0.15 m and backfill thickness is *e*=0.15 m), while Test

49 is a partially buried pipeline in a trench (in which *d*=0.2 m, *e*=0.05 m). For both test cases presented in the figure, the simulated wave height and excess pore-water pressure overall agrees with the collected data in the experiments.

Another comparison is for the normalized amplitude of transient pore-water pressure variation ($|u_e|/p_0$) versus time at various measurement points beneath the pipeline, which are not available in the previous literature (Zhai *et al.*, 2018). As illustrated in Figure 4, the dimensionless amplitude of excess pore pressure profile obtained from in the numerical model (Liang and Jeng, 2018) overall agrees with the experimental data.

4. Results and Discussions

In this study, 71 tests are conducted in total. Among these, Tests 1-40 are primarily performed to investigate the effects of wave parameters (defined in terms of wave height and wave period) on pore pressure in trench layer. Tests 41-71 are mainly conducted to explore the effects of seabed configurations (consisting of backfill thickness as well as trench depth on soil response around a partially backfilled pipeline in the trench. Detailed information of tests is listed in Table 2.

4.1 Effect of wave parameters

To systematically understand the influence of wave parameters on soil responses around a buried pipeline, twenty incident waves, the wave height (*H*) ranging from 0.06 m to 0.14 m with an interval of 0.02 m and the wave period (*T*) varying from 1.2 sec to 1.8 sec with 0.2 sec as a span, are tested for each pipeline-seabed configuration.

Based on the wave and soil characteristics used in the present experiments, transient mechanism dominates the seabed response rather than residual mechanism as reported in Jeng and Seymour (2007) and Jeng (2018). That is, the wave-induced excess pore pressure oscillates periodically and hardly ever accumulates in a sandy seabed. Such phenomena occurred in all experimental tests conducted, which may be ascribed to the fact that the grain size of seabed sediments used in the

present model is too large (d_{50}=0.173 mm) to generate the residual excess pore-water pressure. Therefore, the excess pore pressure induced by the previous wave loading dissipates quickly and fully before the next wave arrives, thus does not accumulate in the sandy seabed.

Figure 5 shows the depth profile of amplitude of normalized excess pore-water pressure ($|u_e|/\sigma_0'$) along the normalized soil depth (z/h) downward from the trench surface to seabed bottom. Here, $\sigma_0' = \gamma' z(1+2K_0)/3$, where K_0 is the coefficient of lateral earth pressure at rest. Compared with the hydrostatic water pressure, the weight of the submarine pipeline is considered to be small, therefore, the effects of pipeline weight on the initial effective stress is ignored as the first approximation. In the figure, the pore-water pressure measured at pipeline bottom corresponds to the value of relative depth z/h=0.357 with the trench depth d=0.2 m and backfill depth e=0.1 m, and three pore pressure transducers are installed at different depths 0.03 m, 0.07 m and 0.20 m (z/h=0.411, 0.482 and 0.714) downward from the trench bottom respectively. Figure 5 shows that the amplitude of excess pore-water pressure attenuates more significantly in the upper layer of the seabed than damps in the lower layer, which is primarily due to the effect of permeability and deformation properties of submarine sediments. Furthermore, a criterion reported by Zen and Yamazaki (1990a) that includes the initial stress due to pre-consolidation is used to determine the oscillatory soil liquefaction, which is well known that soil liquefaction will occur when $|u_e| = \sigma_0'$. The present results indicate that the soil is not liquefied, even with the large wave height and long wave period (e.g., H=0.14 m and T=1.6 sec, or H=0.12 m and T=1.8 sec). Such phenomenon is observed in all tests and could be attributed to the large-size and non-cohesive sediment particles.

Figure 6 presents the vertical distribution of the amplitude of wave-induced excess pore-water pressure with a certain seabed configuration of 2D-depth-trench and 1D-thickness-backfill, for various wave heights. The results reveal that the excess pore-water pressure amplitude increases as the wave height increases, and the amplitude attenuation for the excess pore-water pressure towards the seabed bottom is greater for wave with larger wave height. Besides, the amplitude

of oscillatory pore pressure component recorded at p9 (relative depth *z*/*h*=0.411) is slightly larger than that at p1 (relative depth *z*/*h*=0.357), especially for the cases with larger wave height (e.g., *H*=0.12 m, 0.14 m) and longer wave periods (e.g., *T*=1.6 sec, 1.8 sec). Such a phenomenon differs from the law of monotonous attenuation of pore pressure distribution as the increment of seabed depth without any presence of the pipeline. When a pipeline exists in the submarine environment, the local seepage flow scatter and consequentially the excess pore-water pressure distribution across the soil depth is perturbed. Thus, the energy of the pore pressure within sediments that transferred from wave-induced seafloor pressure, propagates in the neighborhood of the underwater pipeline via several approaches. They might transmit through the soil particles downward directly from the shallow region to the deep layer, or spread along the periphery of the pipeline until reach the pipeline bottom and subsequently downward to the seabed bottom. In the former case, the excess pore-water pressure transmitted through porous media attenuates sharply due to the friction effect and that through the outer circumference of the pipeline definitely dominates the stress distribution, following by the fact that excess pore pressure measured at p9 is smaller than p1. Nevertheless, in the latter case, especially for the wave with longer period and larger height where the damping rate of excess pore-water pressure energy inside the seabed is relatively slight. Therefore, the excess pore pressure delivered by sediment grains and that by outside surface of pipeline has the comparative magnitude. This might lead to the larger value recorded at p9 than p1. More detailed discussions will be provided in the latter section.

Variations of the non-dimensional amplitude of excess pore-water pressure ($|u_e|/p_0$) around the circumferential surface of pipeline under different wave heights are plotted in Figure 7. In these figures, p_0 is the amplitude of dynamic wave pressure at the surface of the mud-line, calculated by the linear wave theory $p_0 = \frac{\gamma_w \mathrm{H}}{2\cosh \mathrm{kd}}$, and the points represent the excess pore pressures ($|u_e|/p_0$), which are measured radially from the center of the circle, with an equal interval of $\pi/4$, where p1 ($\theta = 3\pi/2$), p3 ($\theta = 0$), p5 ($\theta = \pi/2$) and p7 ($\theta = \pi$) corresponding to the bottom, seaward, top, and shoreward edge of the pipeline, respectively (referring to Figure

1). The results presented in the figure are for the case, in which the trench depth of 1.5*D* and backfill thickness of 1.5*D* (the submarine pipeline diameter *D*=0.1 m). Figure 7 demonstrates that the dimensionless amplitude of excess pore-water pressure increases as the wave height increases. The effect of the wave height on excess pore-water pressure presents a positive correlation with the increasing wave height. However, the variation of the transient pore pressure amplitude is insignificant under the wave height generated in this study. In addition, the values of excess pore pressure oscillation measured at the upper half part of the pipeline (e.g., p4, p5, p6) almost have the same magnitude, possessing the largest quantity around the pipeline circumference. Nevertheless, the excess pore pressure oscillatory component recorded at the lower half part (e.g., p1, p2, p8) exhibits the minimum value. This observation is consistent with the conclusion of Pan and Wang (2007), in which the underwater pipeline is fully buried in the sediments with impermeable wall surrounded. That is, in a sandy seabed, higher pore pressure occurs at the pipeline top and the lower pore pressure appears at the bottom.

To further study the effect of wave period (*T*) on the soil dynamic responses around a partially buried pipeline, the case in which the trench depth kept as 2*D* and backfill thickness kept as 1*D* is taken as an example. Figure 8 displays the vertical distribution of the transient excess pore-water pressure recorded along the seabed depth straight beneath the pipeline. As illustrated in these figures, the excess pore pressure around the trenched pipeline increases with the increasing wave period, and generally decays from the surface to the bottom of the seabed. In this study, the water depth remains constant. According to the dispersion relationship of linear wave theory, when the water depth keeps unchanged, the wave with a larger period has a longer wave length. Thus, shorter wave-induced excess pore pressure attenuates faster with depth than that driven by the longer wave (see Figure 8). Moreover, the influences of wave period on the excess pore pressure response decreases as the wave period increases. Taking the case of wave height *H*=0.14 m, for example, the rising percentage of excess pore-water pressure measured at pipeline bottom reaches 33.5%, 20.2%, and 4.5% as the wave period increases from 1.2 sec to 1.4 sec, 1.6 sec and 1.8 sec. That is, the percentage gain of pore pressure declines with the increase of the wave length.

436 The normalized excess pore-water pressure variation around the pipeline circumference plotted
437 in the form of scatter plot with the trench depth of 0.15 m and 0.20 m is represented in Figure 9,
438 under various wave periods. Different from the effect of wave height, the amplitude of excess
439 pore pressure increases considerably with the increase of the wave period. However, the effect
440 of wave period on soil response decreases as wave period increases. This discrepancy is attributed
441 to the fact that the non-dimensional parameter p_0 is calculated by the linear wave theory rather
442 than the recorded data, which are not successfully measured in the experiments. Therefore, the
443 normalized excess pore-water pressure amplitude seems to be insusceptible to the wave height,
444 whereas be susceptible to the wave period. Taking Figure 9(d) as an example, as the wave period
445 increases from 1.2 sec to 1.8 sec, the excess pore-water pressure recorded at p5 increases from
446 0.291 to 0.356, 0.401 and 0.424, leading to the percentage gain of 22.3%, 12.6% and 5.7%.
447 Nevertheless, the dimensionless oscillatory amplitude of pore pressure at the top of the pipeline
448 (recorded by p5) is approximately doubled or even trebled as great as the dimensionless quantity
449 at the bottom (recorded by p1) similarly as Figure 7. Furthermore, under the same incident wave
450 conditions, the magnitude of transient pore pressure measured at p3 (shoreward edge of pipeline)
451 is slightly larger than that at p7 (seaward edge of pipeline). This can be ascribed to the sheltering
452 effect of the submarine pipeline on the energy of wave stress propagating from upstream to
453 downstream, causing the higher liquefaction potential at upstream side of pipeline.

454 **4.2 Effect of backfill thickness**

455 One of main objectives of this study is to explore the effects of backfill thickness and trench depth
456 on the wave-induced pore pressures around a partially buried pipeline, which has no reliable and
457 comprehensive experimental data currently available in the literature.

458 Figure 10 shows the scatter plots of the dimensionless excess pore-water pressure versus various
459 seafloor configurations, including trench depth of (a) d=0.20 m and (b) d=0.15 m with non-backfill
460 gradually increasing to full-backfill (set an interval for backfill thickness as a quarter of the pipeline
461 diameter). The variation of relative buried depth (*e*/*D*) has a significant impact on the variation of

462 excess pore-water pressure($|u_e|/\sigma_0'$). When the submarine pipeline is entirely exposed to water
463 without any protection of backfill deposits, the pore pressure sensors recorded the hydrodynamic
464 pressure, representing almost same magnitude along the upper-periphery of the pipeline. With
465 the existence of overburden sediment, the obtained excess pore-water pressure experiences a
466 sharp decline when the pore pressure sensor is buried into the soil. This damping phenomenon of
467 wave-induced pore pressure oscillation is mainly due to the strong friction effect between soil
468 particles and pore water, which transfers energy from pore fluid to soil grains and attenuates
469 pressure fluctuation. The transient excess pore pressure keeps dropping off as the overburden
470 soil thickness continues to increase, whereas the attenuation degree of the transient excess pore
471 pressure declines. As aforementioned, the criterion of instantaneous liquefaction based on the
472 transient excess pore pressure and the initial vertical effective stress can be expressed as seabed
473 liquefaction will occur when $|u_e| = \sigma_0'$. In general, the seabed in the vicinity of pipeline is more
474 vulnerable to liquefaction as the backfill thickness decreases, as shown in Figure 10. This means
475 that a fully buried pipeline could be better protected against instantaneous seabed liquefaction,
476 compared with a partially backfilled pipeline. These results are consistent with previous research
477 reported by Palmer and King (2008) that compared to a pipe laid in an open trench, the pipe
478 embedded in a trench with sufficient thickness is more insulated from the threat of instability of
479 either the seabed or the pipeline due to the potential liquefaction.

480 In general, a trench layer with partially backfills is typically employed in engineering practice to
481 reduce the financial costs and accelerate the construction process compared to a fully backfilled
482 trench. Therefore, a critical backfill thickness for the resistance to seabed transient liquefaction is
483 urgently required for coastal engineering involved in the design for pipeline project. As sinking of
484 pipelines is a common concern in practical offshore engineering, it is assumed that the pipeline
485 could be completely prevented if there is no liquefaction taking place within the underlying soils.
486 Thus, Figure 10 (a) and (b) demonstrate that the bottom of the pipeline will be unstable and
487 damaged by the oscillatory liquefaction when the backfill thickness is less than 0.5D (i.e., e=0 and
488 e=0.25D). Whereas, this study shows that the partially buried trench will provide the pipeline the

full protection against the oscillatory liquefaction when the backfill thickness is larger than 0.5D.

Figure 11 further presents the effect of relative buried depth (*e*/*D*) on the oscillatory amplitude of excess pore-water pressure($|u_e|/p_0$), measured around the pipeline for the wave height of *H*=0.12 m and wave period of *T*=1.6 sec. The result reveals that the excess pore-water pressure undergoes a either mild or severe decline tendency with increasing relative backfill depth. The excess pore-water pressure at the pipeline bottom begins to decline for relative backfill depth increasing from 0 to 0.25. The excess pore-water pressure at p3 and p7 does not decrease until the relative backfill depth reaches 0.75, while the excess pore pressure at the top of the pipeline starts falling off after the relative backfill depth reaches 1.0. This is because, when the transducer is submerged in water without any presence of buried sediments, the measurement recorded by transducer is the value of wave pressure. However, when the sensor is covered by overburden layer, the measurement recorded by transducer is the value of pore-water pressure instead, which decays along soil depth because of the friction effect between pore water and soil particles within pore seabed. Moreover, the reduction of excess pore-water pressure caused by backfill materials is substantial until the thickness of backfill equals to 1D, while the curve representing the excess pore pressure variation becomes gradual when backfill thickness continues to grow from 1D to 2D. Here, the overburden depth of 1D (0.1 m) is considered to be optimum (minimum) backfill thickness, which is roughly consistent with the experimental results found in Zhai *et al.* (2018).

Figure 12, demonstrated the effect of relative buried depth (*e*/*D*) on the dimensionless excess pore pressure($|u_e|/p_0$) along the soil depth from the pipeline bottom downward to seabed bottom, is examined for the wave condition of *H*=0.12 m and *T*=1.6 sec. Similar to the results around pipeline circumference, the dimensionless excess pore-water pressure decrease as the relative backfill depth increases. However, the decrement at upper layer is larger than that at lower layer.

Figure 13, accompanied with Figure 6 (c), illustrates the systematic depth profiles of normalized excess pore pressure($|u_e|$) versus backfill for the same wave characteristics. The results are for the case in which, the trench depth remains at 0.2 m, whereas the backfill thickness varies from 0

(non-backfill), 0.05 m, 0.1 m, 0.15 m to 0.2 m (full-backfill). As presented in Figure 13, $|u_e|$ measured at p1 (z/h=-0.357) is occasionally smaller than that recorded at p9 (z/h=-0.411), which is inconsistent with the general acknowledgement of decays of excess pore pressure along with soil depth in the absence of a submarine pipeline. These phenomena only occur in the shallow backfill layer under the high-energy wave conditions (i.e., in Figure 12 (a) and (b)). As afore-discussed, wave-induced seafloor pressure is transferred into sediment in terms of pore pressures and its energy propagates downward from the seabed surface to the internal area below the pipeline via diverse approaches, transmitting along the outer surface of the pipeline prior to subsequently downward, and/or passing through the porous bed down primarily. In the case of shallow backfill thickness, where the friction effect is comparatively small, the wave energy delivered by sediment particles and that by external periphery of the pipeline has almost the same magnitude, especially for wave loading with larger wave height or longer wave period. Herein, the larger oscillatory amplitude of the excess pore pressure may be recorded at p9 than that at p1. Nevertheless, when overburden depth is raised to a certain depth, e.g., *e*=0.15 m, 0.2 m, in which the friction effect of porous media cannot be negligible, the transient excess pore pressure transferred through soil grains sharply attenuates and that through the outside circumference of the pipeline definitely dominates the stress field. Thereby, $|u_e|$ measured at p9 is considerably smaller than that at p1, being consistent with the universal rule without the presence of the pipeline.

4.3 Effect of trench depth

Generally speaking, the trench depth has remarkable impacts on the wave-induced soil response in the trench layer around a partially buried pipeline. This is because, that a trench layer definitely perturbs the local flow and soil movement, thus further influence the excess pore pressure in the neighborhood. Duan *et al.* (2018) has numerically investigated that the flow velocity inside the trench is much lower than that outside the trench. In Figure 14, the excess pore-water pressure along the upper-half surface (e.g., $0^\circ < \theta < 180^\circ$) of the pipeline is not considered since the pipeline in some cases (i.e., d=0.05 m and e≤0.05 m when d=0.10 m) is partially buried in the trench

layer. Therefore, only the excess pore-water pressure along the lower-half surface (e.g.,$180^\circ < \theta < 360^\circ$) of the pipeline is discussed, for *H*=0.12 m and *T*=1.6 sec. As shown in Figure 14, the lowest excess pore-water pressure ($|u_e|/\sigma_0'$) occurs at the bottom of the pipeline (measured by p1), while the highest value is located near the trench surface (recorded by p3 and p7). This implies that the upper region around the pipeline is more likely to be liquefied.

Figure 14 further illustrates that excess pore-water pressure generated by wave pressure becomes smaller for larger trench depth. This phenomenon could be ascribed to the fact that the deeper trench means the deeper location of the pipeline below the water surface, where wave-induced excess pore-water pressure will be attenuated more significantly. Therefore, the trench layer with larger depth has greater ability to suppress transient excess pore-water pressure response. As a result, the sheltering effect of the trench becomes stronger. Another observation is that the critical (the minimum) backfill thickness against transient seabed liquefaction for 1.0D-depth trench can be considered as 0.5D, as shown in Figure 14(a). However, even if the 0.5D-depth trench is fully backfilled, the value of excess pore-water pressure ($|u_e|/\sigma_0'$) is greater than 1. This indicates that the 0.5D-depth trench cannot prevent the pipeline from instability and the bottom of the pipeline could be damaged by the wave-induced transient seabed liquefaction.

5. Conclusions

In this paper, a comprehensive experimental investigation on soil responses in the trench layer around a partially backfilled pipeline to cyclic wave loading was reported. Twenty incident wave conditions (in which *H* ranges from 0.06 m to 0.14 m and *T* varies from 1.2 sec to 1.8 sec) are tested in the experiment. Three trench depths (*d*/*D*=1.0, 1.5, 2.0) and corresponding backfill thicknesses, which varies from non-backfill (where *e*/*D*=0) to full-backfill (where *e*/*D*=1.0, 1.5, 2.0 for *d*/*D*=1.0, 1.5, 2.0, respectively), are considered. Note that this is the first set of comprehensive experimental study for the soil response in the vicinity of a partially buried pipeline in a trench layer. Based on the experimental data, the following conclusions can be drawn.

(1) Based on the comparison between the experimental data and the numerical simulation (Liang and Jeng, 2018a,b), both overall agrees in the pore-water pressures along the pipeline periphery and beneath the pipeline for both fully buried (*e*/*D*=0) and partially buried pipelines (*e*/*D*=0.5). The pore pressure closely below the underwater pipeline under large progressive wave loading shows considerable deviation from that predicted by the theoretical model, especially at the lower backfill thickness. This is believed to be caused by the complex seepage flow in the trench layer.

(2) Transient excess pore-water pressure appears as a periodic response to the wave action, significantly determined by the wave characteristics. The oscillation of excess pore pressure presents a left-right circumferential asymmetric distribution, where the seaward edge of the pipeline is more vulnerable to instability caused by potential liquefaction than the shoreward edge. The crest pressure value occurs at the top of the pipeline and the trough pressure takes place at the bottom. The excess pore pressure oscillation in the trench layer attenuates along seabed depth and increase considerably with the increasing wave height and wave period.

(3) Excess pore-water pressure oscillatory amplitude decreases as the thickness of the backfill increases within the range of relative backfill depth chosen in this study. This can be ascribed to the increasing overburden effective stress. For practical engineers involved in the design of offshore pipeline projects, it is vital to determine a critical thickness of the backfill materials to suppress the wave-induced transient seabed liquefaction and meanwhile to reduce the financial budgets. In this study, the backfill thickness of e=0.5D can fully satisfy the requirement of pipeline stability, especially in the deep trench (i.e., d=2.0D and d=1.5D).

(4) Excess pore-water pressure oscillatory amplitude declines as the trench becomes deeper because of the better sheltering effect of trench. However, in the shallower trench, the ability to mitigate excess pore-water pressure becomes weaker as the flow velocity is stronger. Under the wave and soil characteristics tested in this study, the trench layer whose depth is greater than 0.5D could provide a resistance to transient liquefaction occurring at the bottom

of the pipeline.

Acknowledgements

This research was jointly supported by the National Key research and development program of China (2017YFC1404200), the research grants of Jiangsu (BK20150804), the marine renewable energy research project of State Oceanic Administration (GHME2015GC01), Open Foundation of State Key Laboratory of Hydrology-Water Resources and Hydraulic Engineering, Hohai University (Project No: 2016491011), the Royal Academy of Engineering the Distinguished Visiting Fellowship (DVF1718-8-7) and the Fundamental Research Funds for the Central Universities, Hohai University (2016B42514). Comments made by Reviewers have greatly improved the quality of the paper.

Reference:

Allen, D., Lammert, W., Hale, J. and Jacobsen, V. (1989), Submarine pipeline on-bottom stability: recent AGA research, *Proceedings of 21st Annual Offshore Technology Conference,* 1-4 May, 1989, Houston, Texas, OCT6055, 121-132.

Chan, A. H. C. (1988), A unified element solution to static and dynamic problems of geomechanics, PhD thesis, University of Wales Swansea, Wales.

Cheng, A. H. D. and Liu, P. L.-F. (1986), Seepage force on a pipeline buried in a poroelastic seabed under wave loadings, *Applied Ocean Research,* 8(1), 22-32.

Christian, J. T., Taylor, P. K., Yen, J. K. and Erali, D. R.(1974), *Large diameter underwater pipe line for nuclear power plant designed against soil liquefaction*, *Proceedings of Offshore Technology Conference*, 6-8 May, 1974, Houston, Texas, OCT2094, 597–602.

Chowdhury, B., Dasari, G. R. and Nogami, T. (2006), Laboratory study of liquefaction due to wave-seabed interacton, *Journal of Geotechnical and Geoenvironmental Engineering, ASCE*, 132, 841–851.

Damgaard, J. S. and Palmer, A. (2001), Pipeline stability on a mobile and liquefied seabed: A discussion of magnitudes and engineering implications, *Proceedings of the 20th International Conference on Offshore Mechanics and Arctic Engineering, ASME,* Rio de Janeiro, Brazil, 195-204.

619 Damgaard, J. S., Sumer, B. M., Teh, T., Palmer, A., Foray, P. and Osorio, D. (2006), Guidelines for
620 pipeline on-bottom stability on liquefied noncohesive seabeds, *Journal of Waterway, Port,*
621 *Coastal, and Ocean Engineering, ASCE*, 132(4), 300-309.
622 de Groot, M. and Meijers, P. (1992), Liquefaction of trench fill around a pipeline in the seabed,
623 *Proceeding of Conference on the Behavior of Offshore Structures,* London, 1333-1344.
624 Du, X. J. and Zhao, J. (2015), Deep trenching protection of subsea pipeline crossing channel, *Port*
625 *Engineering Technology*, 52(6), 80-83.
626 Duan, L. L., Liao, C. C., Jeng, D.-S. and Chen, L. Y. (2017a), 2D numerical study of wave and current-
627 induced oscillatory non-cohesive soil liquefaction around a partially buried pipeline in a
628 trench, *Ocean Engineering,* 135, 39-51.
629 Duan, L. L., Jeng, D.-S., Liao, C. C., Zhu, B. and Tong, D.G. (2017b), Three-dimensional poro-elastic
630 integrated model for wave and current-induced oscillatory soil liquefaction around an
631 offshore pipeline, *Applied Ocean Research*, 68, 293-306.
632 Dunlap, W., Bryant, W., Williams, G. and Suhayda, J. (1979), Storm wave effects on deltaic
633 sediments – Results of SEASWAB I and II, *Port and Ocean Engineering Under Arctic Conditions*
634 *(POAC79), Norwegian Institute of Technology,* 2, 899-920.
635 Dunn, S. L., Vun, P. L., Chan, A. H. C. and Damgaard, J. S. (2006), Numerical modelling of wave-
636 induced liquefaction around pipelines. *Journal of Waterway, Port, Coastal, and Ocean*
637 *Engineering, ASCE,* 132(4), 276-288.
638 Fredsøe, J. (2016), Pipeline–seabed interaction, *Journal of Waterway, Port, Coastal and Ocean*
639 *Engineering, ASCE,* 142(6), 03116002.
640 Gao, F. P., Gu, X., Jeng, D.-S. and Teo, H. (2002), An experimental study for wave-induced instability
641 of pipelines: The breakout of pipelines, *Applied Ocean Research,* 24(2), 83-90.
642 Gao, F. P., Jeng, D.-S. and Sekiguchi, H. (2003a), Numerical study on the interaction between non-
643 linear wave, buried pipeline and non-homogenous porous seabed, *Computers and*
644 *Geotechnics,* 30(6), 535-547.
645 Gao, F. P., Gu, X. and Jeng, D.-S. (2003b), Physical modeling of untrenched submarine pipeline
646 instability, *Ocean Engineering,* 30(10), 1283-1304.
647 Gao, F. P. and Wu, Y. X. (2006), Non-linear wave-induced transient response of soil around a
648 trenched pipeline, *Ocean Engineering,* 33(3-4), 311-330.
649 Gao, F. P., Yan, S. M., Yang, B. and Wu, Y. (2007), Ocean currents-induced pipeline lateral stability

650 on sandy seabed, *Journal of Engineering Mechanics, ASCE*, 133(10), 1086-1092.
651 Gao, F. P., Yan, S. M., Yang, B. and Luo, C. C. (2011), Steady flow-induced instability of a partially
652 embedded pipeline: pipe–soil interaction mechanism, *Ocean Engineering,* 38(7), 934-942.
653 Herbich, J. B.(1984), *Seafloor scour: Design guidelines for ocean-founded structures*, Marcel Dekker
654 Inc.
655 Jeng, D.-S. (2001), Numerical modeling for wave–seabed–pipe interaction in a non-homogeneous
656 porous seabed, *Soil Dynamics and Earthquake Engineering,* 21(8), 699-712.
657 Jeng, D.-S. (2003), A general finite element model for wave-seabed-structure interaction. In:
658 *Numerical Analysis and Modelling in Geomechanics* (edited by John Bull), Chapter 3, E& FN SPON,
659 London, 59--100.
660 Jeng, D.-S. (2018), *Mechanics of wave-seabed-structure interactions: Modelling, processes and*
661 *application*. Cambridge University Press, Cambridge.
662 Jeng, D.-S. and Lin, Y. S. (1999), Wave-induced pore pressure around a buried pipeline in Gibson
663 soil: Finite element analysis. *International Journal for Numerical and Analytical Methods in*
664 *Geomechanics*, 23 (13), 1559-1578.
665 Jeng, D.-S., Postma, P. and Lin, Y. (2001), Stresses and deformation of buried pipeline under wave
666 loading, *Journal of Transportation Engineering, ASCE, 127*(5), 398-407.
667 Jeng, D.-S. and Seymour, B. R. (2007), Simplified analytical approximation for pore-water pressure
668 buildup in marine sediments, *Journal of Waterway, Port, Coastal, and Ocean Engineering, ASCE,*
669 133(4), 309-312.
670 Liang ZD and Jeng D.-S. (2018a), 3D Numerical model for fluid-seabed interactions around
671 pipelines using OpenFOAM. *Proceedings of the Thirteenth (2018) Pacific-Asia Offshore*
672 *Mechanics Symposium (PACOMS), Jeju, Korea, October 14-17, 2018*, 539-546.
673 Liang ZD and Jeng D.-S. (2018b): A three-dimensional model for the seabed response induced by
674 waves in conjunction with currents in the vicinity of an offshore pipeline using OpenFOAM.
675 *International Journal of Ocean and Coastal Engineering*, accepted
676 Lin, Z. B., Guo, Y. K., Jeng, D.-S., Liao, C. C. and Rey, N. (2016), An integrated numerical model for
677 wave–soil–pipeline interactions, *Coastal Engineering, 108*, 25-35.
678 Liu, B., Jeng, D.-S., Ye, G.L. and Yang, B. (2015), Laboratory study for pore pressures in sandy
679 deposit under wave loading, *Ocean Engineering,* 106, 207-219.

680 Liu B. and Jeng D.-S. (2016), Laboratory study for influence of clay content (CC) on wave-induced
681 liquefaction in marine sediments. *Marine Georesources and Geotechnology*, 34(3), 280-292.
682 Luan, M. T., Qu, P., Jeng, D.-S., Guo, Y. and Yang, Q. (2008), Dynamic response of a porous seabed-
683 pipeline interaction under wave loading: soil-pipe contact effects and inertial effects,
684 *Computers and Geotechnics,* 35(2), 173–86.
685 MacPherson, H. (1978), Wave forces on pipeline buried in permeable seabed, *Journal of Waterway,*
686 *Port, Coastal Ocean Division, ASCE, 104*, 407–419.
687 Magda, W. (1992), Wave-induced pore pressure acting on a buried submarine pipeline, The 23rd
688 International Conference on *Coastal Engineering, ASCE*, 4-9 October, 1992, Venice, Italy,
689 Chapter 240, 3135-3148.
690 Magda, W. (1996), Wave-induced uplift force acting on a submarine buried pipeline: Finite element
691 formulation and verification of computations, *Computers and Geotechnics*, *19*(1), 47-73.
692 McDougal, W. G., Davidson, S. H., Monkmeyer, P. L. and Sollitt, C. K. (1988), Wave-induced forces
693 on buried pipelines, *Journal of Waterway, Port, Coastal, and Ocean Engineering,* ASCE, *114*(2),
694 220-236.
695 Miyamoto, J., Sassa, S. and Sekiguchi, H. (2004), Progressive solidification of a liquefied sand layer
696 during continued wave loading, *Géotechnique,* 54(10), 617-629.
697 Monkmeyer, P. L., Mantovani, P. and Vincent, H. (1983), Wave-induced seepage effects on a buried
698 pipeline, *Proceeding of Coastal Structures'83*, *ASCE*, 519-531.
699 Okusa, S. (1985), Wave-induced stresses in unsaturated submarine sediments, *Géotechnique*, 35,
700 517-532.
701 Palmer, A. C., Steenfelt, J., Steensen-Bach, J. and Jacobsen, V. (1988), Lateral resistance of marine
702 pipelines on sand, *Proceedings of 20th Annual Offshore Technology Conference,* 2-5 May,
703 Houston, Texas, OCT5853, 399-408.
704 Palmer, A. C. and King, R. A. (2004), *Subsea pipeline engineering*, PennWell, Oklahoma.
705 Pan, D. Z., Wang, L. Z., Pan,C. H. and Hu, J. C. (2007), Experimental investigation on the wave-
706 induced pore pressure around shallowly embedded pipelines, *Acta Oceanologica Sinica*, 26(5),
707 125-135.
708 Sassa, S. and Sekiguchi, H. (1999), Wave-induced liquefaction of beds of sand in a centrifuge,
709 *Géotechnique*, 49(5), 621-638.
710 Sassa, S. and Sekiguchi, H. (2001), Analysis of wave-induced liquefaction of sand beds,

711 *Géotechnique*, 51(2), 115–26.
712 Sudhan, C. M., Sundar, V. and Rao, S. N. (2002), Wave induced forces around buried pipelines,
713 *Ocean Engineering,* 29(5), 533-544.
714 Sumer, B. M., Fredsøe, J., Christensen, S. and Lind, M. (1999), Sinking/floatation of pipelines and
715 other objects in liquefied soil under waves, *Coastal Engineering, 38*(2), 53-90.
716 Sumer, B. M., Hatipoglu, F., Fredsøe, J. and Hansen, N.-E. O. (2006), Critical flotation density of
717 pipelines in soils liquefied by waves and density of liquefied soils, *Journal of Waterway, Port,*
718 *Coastal, and Ocean Engineering,* ASCE, *132*(4), 252-265.
719 Sumer, B. M. (2014a), Flow–structure–seabed interactions in coastal and marine environments,
720 *Journal of Hydraulic Research*, 52(1), 1-13.
721 Sumer, B. M. (2014b), Advances in seabed liquefaction and its implications for marine structures,
722 *Geotechnical Engineering*, 45(4), 1-14.
723 Sumer, B. M. (2014c), *Liquefaction around marine structures*, *World Scientific*, Singapore.
724 Teh, T., Palmer, A. and Damgaard, J. S. (2003), Experimental study of marine pipelines on unstable
725 and liquefied seabed, *Coastal Engineering, 50*(1-2), 1-17.
726 Teh, T., Palmer, A., Bolton, M. and Damgaard, J. S. (2006), Stability of submarine pipelines on
727 liquefied seabeds, *Journal of Waterway, Port, Coastal, and Ocean Engineering,* ASCE, *132*(4), 244-
728 251.
729 Turcotte, B. R., Kulhawy, F. H. and Liu, P. L. (1984), *Laboratory evaluation of wave tank parameters*
730 *for wave-sediment interaction*, Technical Report 84-1, Joseph F. Defree Hydraulic Laboratory,
731 School of Civil and Environmental Engineering, Cornell University.
732 Wang, X., Jeng, D.-S. & Lin, Y. S. (2000), Effects of a cover layer on wave-induced pore pressure
733 around a buried pipe in an anisotropic seabed, *Ocean Engineering,* 27(8), 823–39.
734 Yang, L. P., Shi, B., Guo, Y. K. and Wen, X., (2012a), Calculation and experiment on scour depth for
735 submarine pipeline with a spoiler. *Ocean Engineering,* 55, 191–198.
736 Yang, L. P., Guo, Y. K., Shi, B., Kuang, C. P., Xu, W. L. and Cao, S., (2012b), Study of scour around
737 submarine pipeline with a rubber plate or rigid spoiler in wave conditions. *Journal of Waterway,*
738 *Port, Coastal Ocean Engineering, ASCE*, 138, 484–490.
739 Yang, L. P., Shi, B., Guo, Y. K., Zhang, L. X., Zhang, J. S. and Han, Y. (2014), Scour protection of
740 submarine pipelines using rubber plates underneath the pipes, *Ocean Engineering*, 84, 176-182.
741 Zen, K. and Yamazaki, H. (1990a), Mechanism of wave-induced liquefaction and densification in

seabed, *Soils and Foundations,* 30(4), 90–104.

Zen, K. and Yamazaki, H. (1990b), Oscillatory pore pressure and liquefaction in seabed induced by ocean waves, *Soils and Foundations*, 30(4), 147–61.

Zhai, Y. Y., He, R., Zhao, J., Zhang, J.-S., Jeng, D.-S. and Li, L. (2018), Physical Model of wave-induced seabed response around trenched pipeline in sandy seabed, *Applied Ocean Research, 75*, 37-52.

Zhao, H. Y. and Jeng, D.-S. (2014), Numerical study for wave-induced pore pressure accumulations around buried pipeline: effects of back-filled trench layer, *The 14th International Conference of the International Association for Computer Methods and Advances in Geomechanics (14IACMAG)*, Kyoto, Japan, 1113–18.

Zhao, H. Y., Jeng, D.-S., Guo, Z. and Zhang, J.-S. (2014), Two-dimensional model for pore pressure accumulations in the vicinity of a buried pipeline, *Journal of Offshore Mechanics and Arctic Engineering, ASME, 136*(4), 042001.

Zhao, H. Y. and Jeng, D.-S. (2016), Accumulated Pore Pressures around Submarine Pipeline Buried in Trench Layer with Partial Backfills, *Journal of Engineering Mechanics,* ASCE, *142*(7), 04016042.

Zhou, C. Y., Li, G. X., Dong, P., Shi, J. H. and Xu, J. S. (2011), An experimental study of seabed responses around a marine pipeline under wave and current conditions, *Ocean Engineering, 38*(1), 226-234.

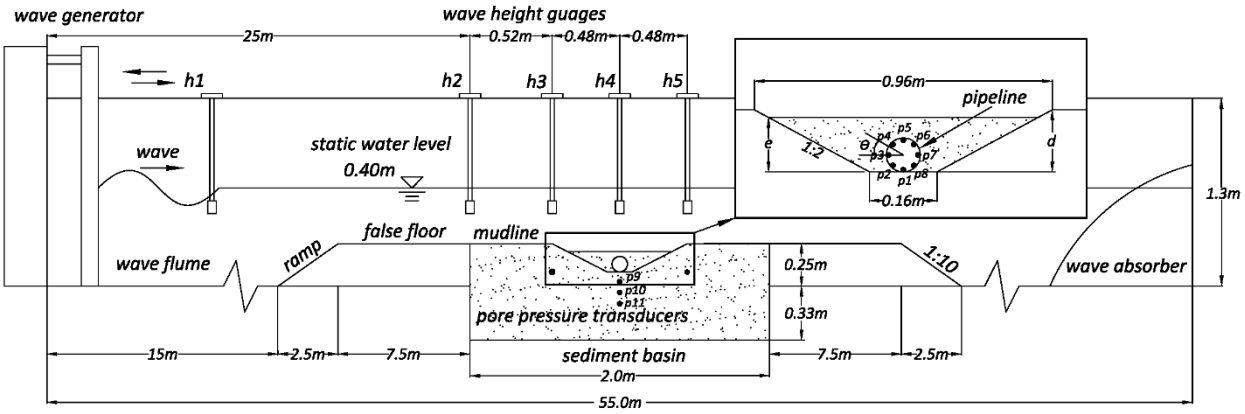

760

761 Fig 1

762

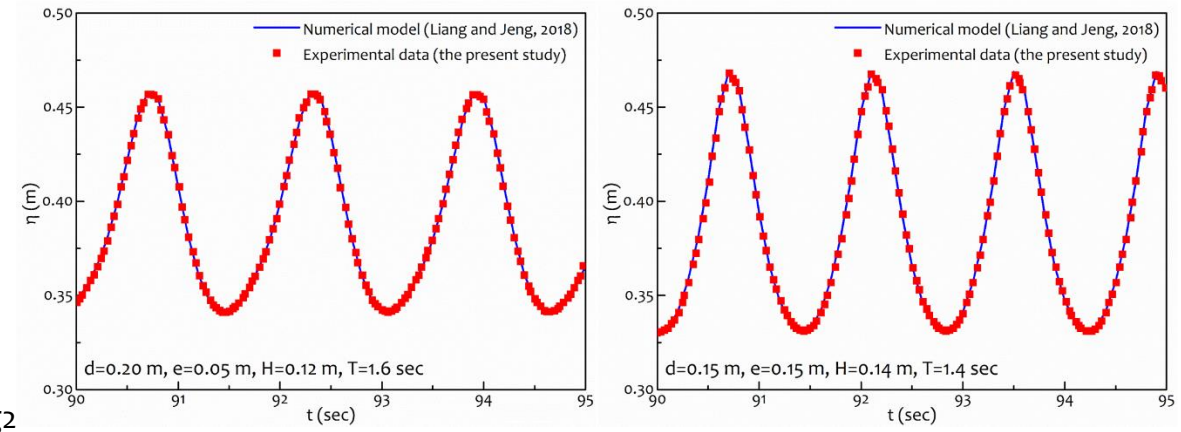

763 Fig2

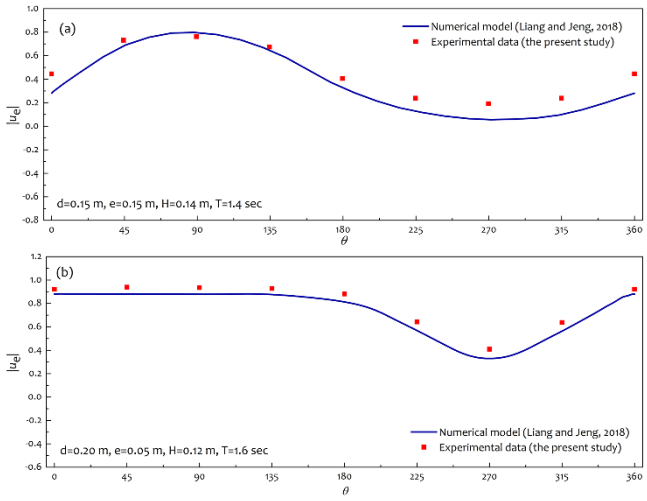

764

765 Fig3

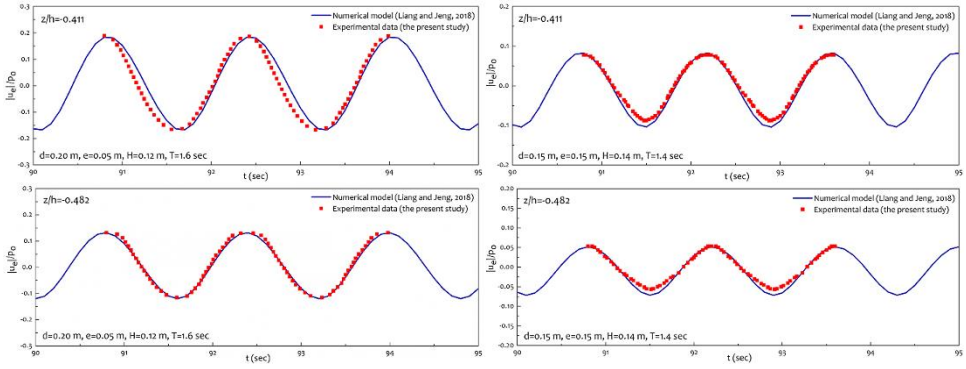

766

767 Fig4

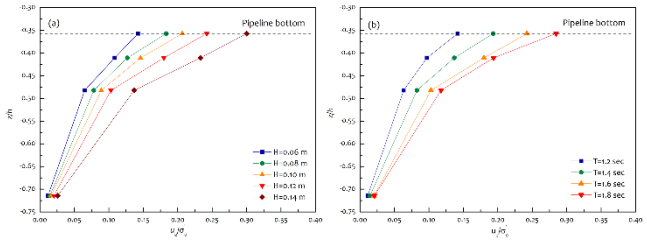

768

769 Fig 5

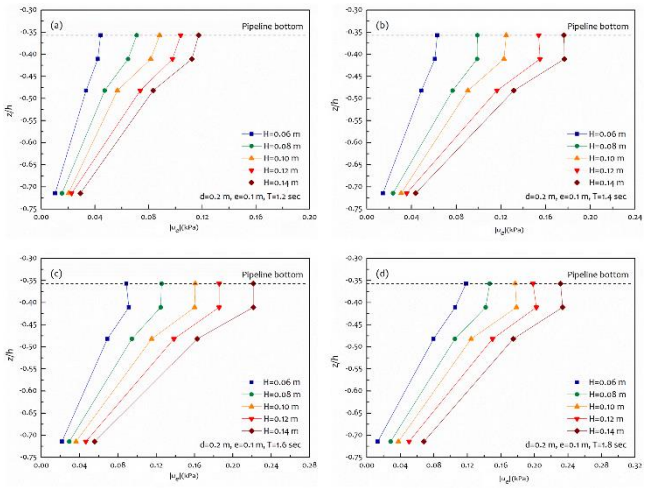

770

771 Fig6

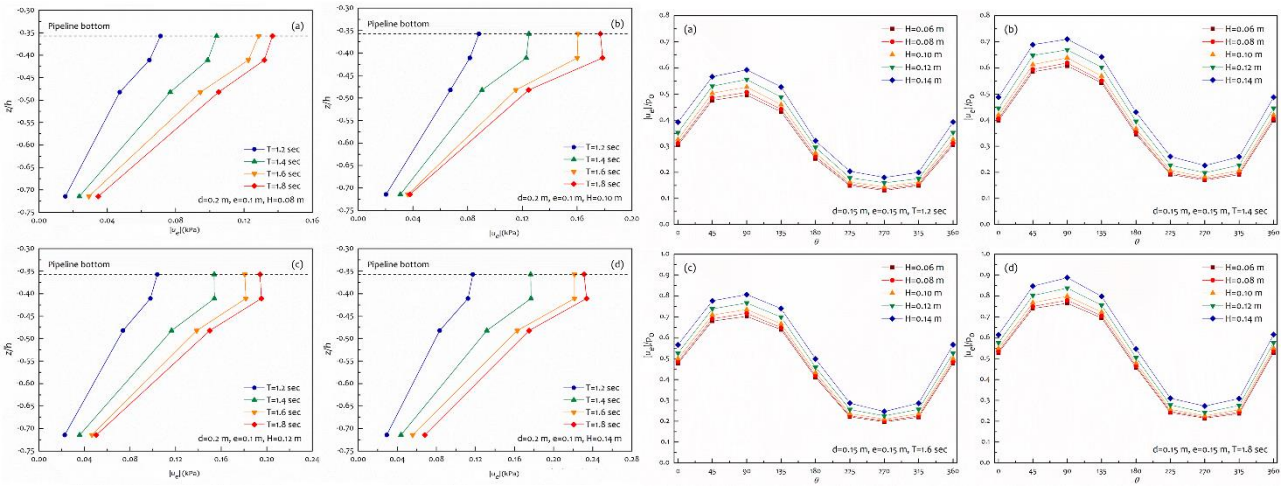

772

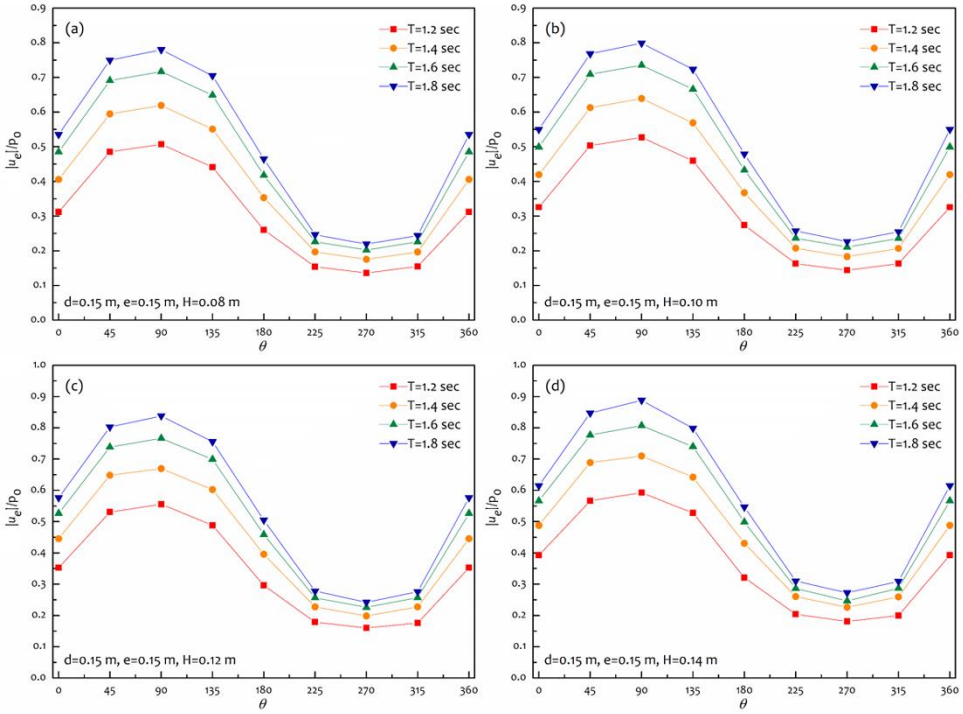

773

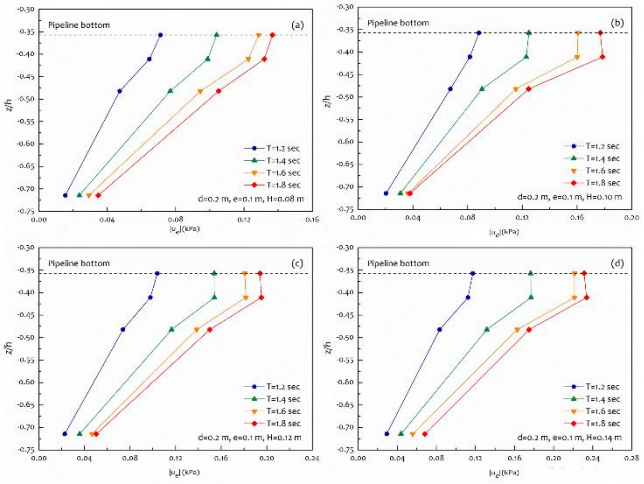

774

775 Fig 7,8,9

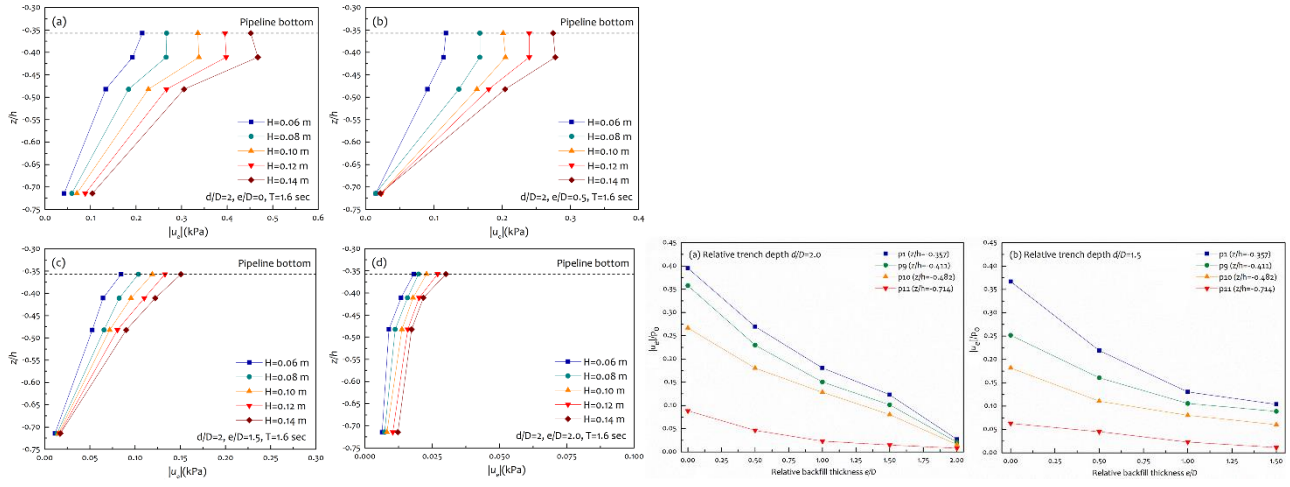

776

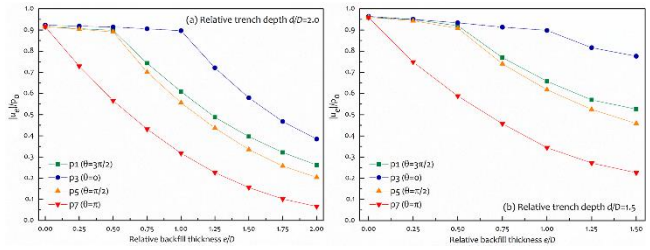

777

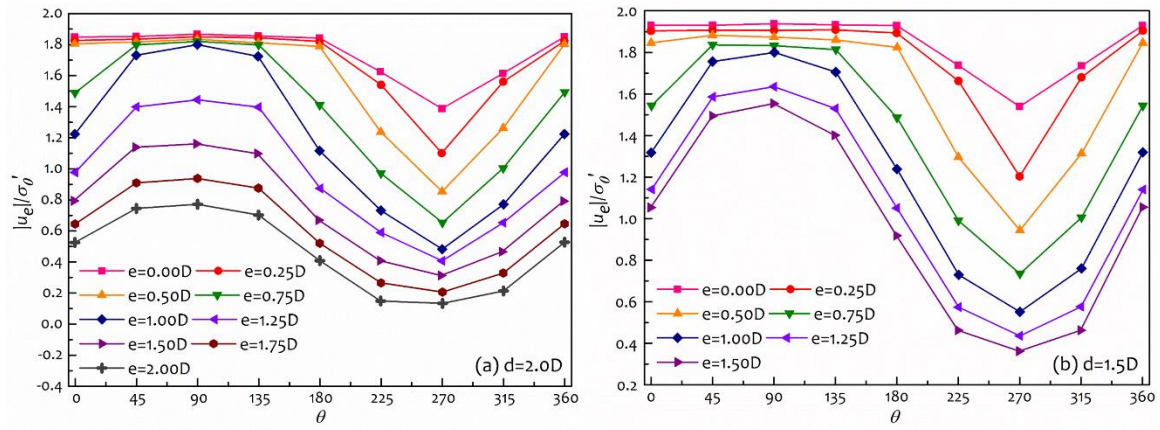

778

779

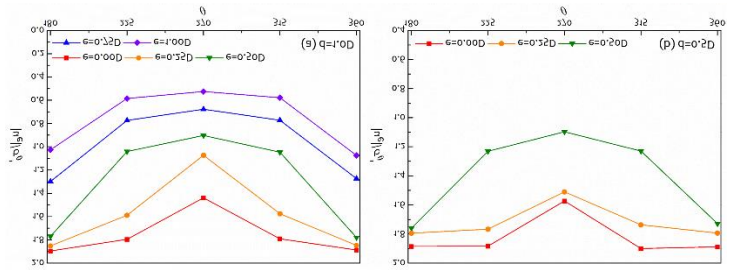

780

781 Fig 10-14

782

783 **Figure captions:**

784 Figure 1 Sketch of the wave flume and experimental setup.

785 Figure 2 Comparison of the simulated and measured water surface elevation recorded by wave height gauge
786 h4, for (a) Test 10 and (b) Test 49.

787 Figure 3 Comparison of the simulated and measured circumferential distribution of the oscillatory excess pore-
788 water pressure amplitude ($|u_e|/p_0$) along the periphery of the pipeline against numerical solution (Liang
789 and Jeng, 2018): (a) Test 10 and (b) Test 49.

790 Figure 4 Comparison of the simulated and measured vertical distribution of the oscillatory excess pore-water
791 pressure amplitude ($|u_e|/p_0$) through the center of the pipeline against numerical solution (Liang and Jeng,
792 2018): (a) Test 10 and (b) Test 49.

793 Figure 5 Effect of (a) wave height and (b) wave period on the distribution of the ratio between the oscillatory
794 excess pore-water pressure amplitude and the initial effective stress ($|u_e|/\sigma_0'$) along the vertical line below
795 pipeline bottom versus relative depth (*z*/*h*) under different incident waves.

796 Figure 6 Distribution of oscillatory amplitude of wave-induced excess pore-water pressure ($|u_e|$) near the wave
797 troughs along the central axis at four positions below the pipeline, *z*=0.20 m (p1), 0.23 m (p9), 0.27 m (p10)
798 and, 0.40 m (p11), for various wave heights. (a) *T*=1.2 sec, (b) *T*=1.4 sec, (c) *T*=1.6 sec, and (d) *T*=1.8 sec.

799 Figure 7 Distribution of non-dimensional amplitude of wave-induced excess pore pressure ($|u_e|/p_0$), around the
800 pipeline outer-surface recorded by p1 to p8, for various wave heights. (a) *T*=1.2 sec, (b) *T*=1.4 sec, (c) *T*=1.6
801 sec, and (d) *T*=1.8 sec.

802 Figure 8 Distribution of oscillatory amplitude of wave-induced excess pore-water pressure ($|u_e|$) near the wave
803 troughs along the central axis at four position below the pipeline, *z*=0.20 m (p1), 0.23 m (p9), 0.27 m (p10)
804 and, 0.40 m (p11), for various wave periods. (a) *H*=0.08 m, (b) *H*=0.10 m, (c) *H*=0.12 m, and (d) *H*=0.14 m.

805 Figure 9 Distribution of non-dimensional amplitude of wave-induced excess pore pressure ($|u_e|/p_0$), around the
806 pipeline outer-circumference recorded by p1 to p8, for various wave periods.
807 Figure 10 Scatter plot of normalized amplitude of excess pore pressure ($|u_e|/\sigma_0'$) around pipeline circumference,
808 under wave height *H*=0.12 m and wave period *T*=1.6 sec, for various backfill thickness: (a) backfill depth (d)
809 ranging from 0.00*D* to 2.00*D* with an interval of 0.25*D*, trench depth *e*=2.0*D*; (b) backfill depth (d) ranging
810 from 0.00*D* to 1.50*D* with an interval of 0.25*D*, trench depth *e*=1.5*D*.
811 Figure 11 Variation of dimensionless amplitude of excess pore pressure ($|u_e|/p_0$) along the pipeline periphery at
812 p1 ($\vartheta=3\pi/2$), p3 ($\vartheta=0$), p5 ($\vartheta=\pi/2$) and p7 ($\vartheta=\pi$) for *H*=0.12 m and *T*=1.2 sec, under different seabed patterns:
813 (a) *d*=2.0*D*, *e*/*D* ranging from 0 to 2.00; (b) *d*=1.5*D*, *e*/*D* ranging from 0 to 1.50.
814 Figure 12 Variation of dimensionless amplitude of excess pore-water pressure ($|u_e|/p_0$) along the central
815 vertical line downward recorded at p1 (*z*/*h*=0.357), p9 (*z*/*h*=0.411), p10 (*z*/*h*=0.482), and p11 (*z*/*h*=0.714) for
816 wave height *H*=0.12m and wave period *T*=1.2 s. These results are for the case in which trench depth *d*=2.0*D*
817 with various backfill depth, and the interval of backfill depth is 0.5*D*.
818 Figure 13 Distribution of normalized excess pore-water pressure versus backfill thickness
819 Figure 14 Scatter plot of normalized amplitude of excess pore pressure ($|u_e|/\sigma_0'$) around pipeline circumference,
820 under wave height *H*=0.12 m and wave period *T*=1.6 sec, for various trench depth: (a) trench depth *e*=1.0*D*;
821 (b) trench depth *e*=0.5*D*.
822
823 Table 1 Soil properties

Parameter	Symbol	Value
Mean grain size	$d_{50}(\mathrm{mm})$	0.173
Unit weight of soil	$\gamma_s(\mathrm{kN/m^3})$	26.5

Submerged unit weight of soil	$\gamma'(\mathrm{kN/m^3})$	19.7
Specific gravity of sediment grain	$G_s = \gamma_s/\gamma_w$	2.70
Permeability	k (m/s)	3.56×10^{-5}
Poisson's ratio	μ	0.32
Maximum void ratio	$e_{\max}$	0.886
Minimum void ratio	$e_{\min}$	0.420
Void ratio	e_s	0.564
Porosity	n	0.396
Relative density	$D_r = \dfrac{e_{\max} - e_s}{e_{\max} - e_{\min}}$	0.624

824

825 Table 2 Experiment conditions

Case	Wave condition		Seabed condition	
No.	Wave height *H* (m)	Wave period *T* (sec)	Trench depth *d* (m)	Backfill depth *e* (m)
1	0.06	1.2	0.15	0.15
2	0.08	1.2	0.15	0.15
3	0.10	1.2	0.15	0.15
4	0.12	1.2	0.15	0.15
5	0.14	1.2	0.15	0.15
6	0.06	1.4	0.15	0.15
7	0.08	1.4	0.15	0.15
8	0.10	1.4	0.15	0.15
9	0.12	1.4	0.15	0.15
10	0.14	1.4	0.15	0.15
11	0.06	1.6	0.15	0.15
12	0.08	1.6	0.15	0.15
13	0.10	1.6	0.15	0.15
14	0.12	1.6	0.15	0.15

15	0.14	1.6	0.15	0.15
16	0.06	1.8	0.15	0.15
17	0.08	1.8	0.15	0.15
18	0.10	1.8	0.15	0.15
19	0.12	1.8	0.15	0.15
20	0.14	1.8	0.15	0.15
21	0.06	1.2	0.20	0.20
22	0.08	1.2	0.20	0.20
23	0.10	1.2	0.20	0.20
24	0.12	1.2	0.20	0.20
25	0.14	1.2	0.20	0.20
26	0.06	1.4	0.20	0.20
27	0.08	1.4	0.20	0.20
28	0.10	1.4	0.20	0.20
29	0.12	1.4	0.20	0.20
30	0.14	1.4	0.20	0.20
31	0.06	1.6	0.20	0.20
32	0.08	1.6	0.20	0.20
33	0.10	1.6	0.20	0.20
34	0.12	1.6	0.20	0.20
35	0.14	1.6	0.20	0.20
36	0.06	1.8	0.20	0.20
37	0.08	1.8	0.20	0.20
38	0.10	1.8	0.20	0.20
39	0.12	1.8	0.20	0.20
40	0.14	1.8	0.20	0.20
41	0.12	1.6	0.15	0
42	0.12	1.6	0.15	0.025

43	0.12	1.6	0.15	0.05
44	0.12	1.6	0.15	0.075
45	0.12	1.6	0.15	0.1
46	0.12	1.6	0.15	0.125
47	0.12	1.6	0.20	0
48	0.12	1.6	0.20	0.025
49	0.12	1.6	0.20	0.05
50	0.12	1.6	0.20	0.075
51	0.12	1.6	0.20	0.1
52	0.12	1.6	0.20	0.125
53	0.12	1.6	0.20	0.15
54	0.12	1.6	0.20	0.175
55	0.08	1.6	0.20	0
56	0.10	1.6	0.20	0
57	0.12	1.6	0.20	0
58	0.14	1.6	0.20	0
59	0.08	1.6	0.20	0.05
60	0.10	1.6	0.20	0.05
61	0.12	1.6	0.20	0.05
62	0.14	1.6	0.20	0.05
63	0.08	1.6	0.20	0.15
64	0.10	1.6	0.20	0.15
65	0.12	1.6	0.20	0.15
66	0.14	1.6	0.20	0.15
67	0.08	1.6	0.20	0.20
68	0.10	1.6	0.20	0.20
69	0.12	1.6	0.20	0.20
70	0.14	1.6	0.20	0.20

71	0.12	1.6	0.10	0.1

826
827